Sciencexpress Reports

Probing Johnson noise and ballistic transport in normal metals with a single-spin qubit

S. Kolkowitz,[1*] A. Safira,[1*] A. A. High,[1,2] R. C. Devlin,[2] S. Choi,[1] Q. P. Unterreithmeier,[1] D. Patterson,[1] A. S. Zibrov,[1] V. E. Manucharyan,[3] H. Park,[1,2†] M. D. Lukin[1†]

[1]Department of Physics, Harvard University, Cambridge, MA 02138, USA. [2]Department of Chemistry and Chemical Biology, Harvard University, Cambridge, MA 02138, USA. [3]Department of Physics, University of Maryland, College Park, MD 20742, USA.

*These authors contributed equally to this work.

†Corresponding author. E-mail: lukin@physics.harvard.edu (M.D.L.); hongkun_park@harvard.edu (H.P.)

Thermally induced electrical currents, known as Johnson noise, cause fluctuating electric and magnetic fields in proximity to a conductor. These fluctuations are intrinsically related to the conductivity of the metal. We use single spin qubits associated with nitrogen-vacancy centers in diamond to probe Johnson noise in the vicinity of conductive silver films. Measurements of polycrystalline silver films over a range of distances (20-200 nm) and temperatures (10-300 K) are consistent with the classically expected behavior of the magnetic fluctuations. However, we find that Johnson noise is dramatically suppressed next to single-crystal films, indicative of a substantial deviation from Ohm's law at length scales below the electron mean free path. Our results are consistent with a generalized model that accounts for the ballistic motion of electrons in the metal, indicating that under the appropriate conditions nearby electrodes may be used for controlling nanoscale optoelectronic, atomic and solid-state quantum systems.

Understanding electron transport, dissipation, and fluctuations at sub-micron length scales is critical for the continued miniaturization of electronic (*1*, *2*) and optical devices (*3–5*), as well as atom and ion traps (*6–10*), and for the electrical control of solid-state quantum circuits (*11*). While it is well known that electronic transport in small samples defies the conventional wisdom associated with macroscopic devices, resistance-free transport is difficult to observe directly. Most of the measurements demonstrating these effects make use of ohmic contacts attached to sub-micron scale samples and observe quantized but finite resistance corresponding to the voltage drop at the contact of such a system with a macroscopic conductor (*12*, *13*). Techniques for non-invasive probing of electron transport are now actively explored (*14*, *15*) because they can provide insights into electronic dynamics at small length scales. Our approach makes use of the electromagnetic fluctuations associated with Johnson noise close to a conducting surface, which can be directly linked to the dielectric function at similar length scales, providing a non-invasive probe of electronic transport inside the metal. Measurements of these fluctuations at micron length scales utilizing cold, trapped atoms showed excellent agreement with predictions based on diffusive electron motion (*7–9*), while millimeter length scale measurements utilizing superconducting quantum interference devices (SQUIDs) have been demonstrated for use as an accurate, contact free thermometer (*16*).

Our approach makes use of the electronic spin associated with nitrogen-vacancy defect centers in diamond (NVs) to study the spectral, spatial, and temperature dependence of Johnson noise emanating from conductors. The magnetic Johnson noise results in a reduction of the spin lifetime of individual NV electronic spins, thereby allowing us to probe the intrinsic properties of the conductor non-invasively over a wide range of parameters. Individual, optically resolvable, NV centers are implanted ~15 nm below the surface of a ~30-μm thick diamond sample. A silver film is then deposited or positioned on the diamond surface (Fig. 1A). The spin sublevels $|ms=0\rangle$ and $|ms=\pm1\rangle$ of the NV electronic ground state exhibit a zero-field splitting of $\Delta = 2\pi\times 2.88$ GHz (*17–20*). The relaxation rates between the $|0\rangle$ and $|\pm1\rangle$ states provide a sensitive probe of the magnetic field noise at the transition frequencies $\omega = \Delta \pm 2g\mu_B B_{\|}$, where $B_{\|}$ is the magnetic field along the NV axis (*21*, *22*) (Fig. 1B).

The impact of Johnson noise emanating from a polycrystalline silver film deposited on the diamond surface (Fig. 1C) is evident when comparing the relaxation of a single NV spin below the silver (red circles) to the relaxation of the same NV prior to film deposition and after removal of the silver (open blue squares and triangles, respectively). At room temperature and in the absence of external noise, the spin lifetime is limited by phonon-induced relaxation to $T_1^{ph} \approx 4$ ms. With the silver nearby, the lifetime of the $|ms=0$ state is reduced to $T_1 = 165$ μs, which we attribute to magnetic Johnson noise emanating from the film. To verify that the enhanced relaxation is due to magnetic noise, we compare the lifetime of the $|0\rangle$ state, which has magnetic dipole

allowed transitions to both of the $|\pm1\rangle$ states, to that of the $|-1\rangle$ state, which can only decay directly to the $|0\rangle$ state (Fig. 1D). As expected for relaxation induced by magnetic noise, the $|-1\rangle$ state has approximately twice the lifetime of the $|0\rangle$ state (*23*). This is in contrast to the observed lifetimes when limited by phonon-induced relaxation (Inset, Fig. 1D), where the $|0\rangle$ and $|\pm1\rangle$ states have almost identical lifetimes (*24*). In what follows we define T_1 as the lifetime of the $|ms=0\rangle$ state.

To test the scaling of Johnson noise with distance (d) to the metal, we deposit a layer of SiO_2 on the diamond surface with a gradually increasing thickness (Fig. 2A). We characterize the thickness of the SiO_2 layer as a function of position on the sample (Inset, Fig. 2B), and deposit a 60-nm polycrystalline silver film on top of the SiO_2. The conductivity of the silver film is measured to be 2.9×10^7 S/m at room temperature. By measuring the relaxation rates $\Gamma=1/T_1$ of individual NVs at different positions along the SiO_2 ramp we extract the distance dependence of the noise (Fig. 2B), with the uncertainty in the distance dominated by the variation in the implanted depth of the NVs (taken to be 15 ± 10 nm). To ensure that the measured rates are Johnson noise limited, we measure the spin relaxation of 5-10 randomly selected NVs per location along the ramp, and plot the minimum observed rate at each location (*23*). As expected (*7–9*), the magnitude of the noise increases as the NVs approach the silver surface.

To investigate the dependence of the noise on temperature and conductivity, we deposit a 100-nm polycrystalline silver film on a diamond sample and measure the T_1 of a single NV beneath the silver over a range of temperatures (~10-295 K). The measured relaxation rate for a single NV near the silver increases with temperature (red circles in Fig. 3A), as expected for thermal noise, but the scaling is clearly non-linear. This can be understood by recognizing that the conductivity of the silver film is also a function of temperature, and that the magnitude of the thermal currents in the silver depend on the conductivity. To account for this effect, a four point resistance measurement of the silver film is performed to determine the temperature dependence of the bulk conductivity of the silver film (Fig. 3B).

To analyze the dependence of the NV spin relaxation rate on distance, temperature, and conductivity, the model of ref. (*6*) is used, in which an electronic spin-1/2 qubit with Larmor frequency ω_L is positioned at a distance d from the surface of a metal. For silver at room temperature the skin depth at ω_L is $\delta\approx1$ μm; consequently when $d<100$ nm we are in the "quasi-static" limit $d\ll\delta$. The thermal limit $k_BT\gg\hbar\omega_L$ is valid for all temperatures in this work. In this regime the magnetic noise spectral density perpendicular to the silver surface is given by

$$S_B^z=\frac{\mu_0^2}{16\pi}\frac{k_BT\sigma}{d}, \qquad (1)$$

where σ is the temperature-dependent conductivity of the metal as defined by the Drude model. This scaling can be intuitively understood by considering the magnetic field generated by a single thermal electron in the metal at the NV position, $B_0=\frac{\mu_0 e v_{th}}{4\pi d^2}$, where the thermal velocity $v_{th}\propto\sqrt{k_BT/m_e}$, m_e is the effective mass of electrons in silver and e is the electron charge. In the limit $d\ll\delta$ screening can be safely ignored, and the NV experiences the magnetic field spectrum arising from N independent electrons in a volume V, $S_B\propto Vn\langle B_0\rangle^2\tau_c$, where n is the electron density and τc is the correlation time of the noise, given by the average time between electron scattering events, $\tau_c=l/v_F$, where l is the electron mean free path and v_F is the Fermi velocity. Recognizing that the NV is sensitive to the motion of electrons within a sensing volume $V\propto d^3$, we arrive at the scaling given by Eq. 1, with $\sigma=\frac{ne^2\tau_c}{m_e}$. Applying Fermi's golden rule and accounting for the orientation and spin-1 of the NV yields the relaxation rate for the $|ms=0\rangle$ state

$$\Gamma=\frac{1}{T_1}=\frac{3g^2\mu_B^2}{2\hbar^2}S_B^z\left(1+\frac{1}{2}\sin^2(\theta)\right), \qquad (2)$$

where $g\approx2$ is the electron g-factor, μ_B is the Bohr magneton, and $\theta\approx54.7^\circ$ is the angle of the NV dipole relative to the surface normal vector (*23*). In Fig. 2B the inverse scaling with distance d predicted by Eq. 1 is clearly evident for NVs very close to the silver. At distances comparable to the silver film thickness Eq. 1 is no longer valid, but we recover excellent agreement with the no-free-parameters prediction of Eq. 2 by including a correction for the thickness of the silver film (red dashed line in Fig. 2B), which is measured independently. The measured relaxation rates as a function of temperature are also in excellent agreement with the predictions of Eq. 2 (red dashed line in Fig. 3A), while the extracted distance of 31 ± 1 nm is consistent with the expected depth (*23*).

Remarkably, very different results are obtained when we replace the polycrystalline film with single-crystal silver. For this experiment, a 1.5-μm thick single-crystal silver film grown by sputtering onto silicon (*23*, *25*, *26*) is placed in contact with the diamond surface. The measured conductivity of the single-crystal silver exhibits a much stronger temperature dependence (blue line in Fig. 4A) as compared to that of the 100-nm thick polycrystalline film. Figure 4B presents the measured relaxation rate as a function of temperature for an NV in a region in direct contact with the single-crystal silver (blue squares). The dashed blue line corre-

sponds to the temperature dependent rate predicted by Eq. 2, which strongly disagrees with the experimental results. Specifically, because the measured silver conductivity increases faster than the temperature decreases in the range from room temperature down to 40 K, Eq. 2 predicts the relaxation rate should increase as the temperature drops, peaking at 40 K and then dropping linearly with temperature once the conductivity saturates. Instead, the T_1 of the NV consistently increases as the temperature drops, implying that at lower temperatures the silver produces considerably less noise than expected from Eq. 2. We observe similar deviation from the prediction of Eq. 2 for all 23 NVs measured in the vicinity of the single-crystal silver (*23*).

To analyze these observations, we note that the conventional theoretical approach (*6*) resulting in Eq. 2 treats the motion of the electrons in the metal as entirely diffusive, using Ohm's law, $\mathbf{J}(\mathbf{r},t)=\sigma\mathbf{E}(\mathbf{r},t)$, to associate the bulk conductivity of the metal with the magnitude of the thermal currents. While accurately describing the observed relaxation rates next to the polycrystalline material, where the resistivity of the film is dominated by electron scattering off of grain boundaries (Inset, Fig. 3B), this assumption is invalid in the single-crystal silver film experiments, particularly at low temperatures. Here, the measured conductivity of the single-crystal film indicate that the mean free path l is greater than one micron, significantly exceeding the sensing region determined by the NV-metal separation, and thus the ballistic motion of the electrons must be accounted for. Qualitatively, the correlation time of the magnetic noise in this regime is determined by the ballistic time of flight of electrons through the relevant interaction region $\tau c \sim d / v_F$ (Fig. 4C). This results in a saturation of the noise spectral density and the spin relaxation rate Γ as either the NV approaches the silver surface or as the mean free path becomes longer at lower temperatures (*23*), with the ultimate limit to the noise spectrum given by:

$$S_B^z = \frac{2}{\pi}\mu_0^2 k_B T \frac{ne^2}{m_e v_F}. \qquad (3)$$

This regime of magnetic Johnson noise was recently analyzed theoretically (*11*) using the Lindhard form non-local dielectric function for the metal modified for finite electron scattering times (*23*, *27*, *28*). Comparison of this model (solid line in Fig. 4B) to the data, with distance again as the only free parameter, yields excellent agreement for all 23 measured NVs (*23*). Fig. 4D shows the measured T_1 times at 103 K and 27 K for each NV as a function of extracted distance (blue triangles). Of the 23 NVs measured, 15 are in a region of the diamond sample in direct contact with the silver (*23*). Excellent agreement between the non-local model (solid lines) and the data is observed for all 23 NVs at all 12 measured temperatures. Apparent in Fig. 4D is the saturation of the relaxation rate as the NV approaches the silver surface, and as the mean free path becomes longer at lower temperatures (dashed black line), as predicted by Eq. 3.

While ballistic electron motion in nanoscale structures has previously been studied and utilized (*12*, *13*), our approach allows for non-invasive probing of this and related phenomena, and provides the possibility for studying mesoscopic physics in macroscopic samples. The combination of sensitivity and spatial resolution demonstrated here enables direct probing of current fluctuations in the proximity of individual impurities, with potential applications such as imaging of Kondo states and probing of novel two-dimensional materials (*29*), where our technique may allow for the spatially resolved probing of edge states (*12*). Likewise, it could enable investigation of the origin of $1/f$ flux noise by probing magnetic fluctuations near superconducting Josephson circuits (*30*, *31*). Finally, as Johnson noise presents an important limitation to the control of classical and quantum mechanical devices at small length scales (*6*–*10*), the present results demonstrate that this limitation can be circumvented by operating below the length scale determined by the electron mean free path.

REFERENCES AND NOTES

1. M. Lundstrom, Applied physics. Moore's law forever? *Science* **299**, 210–211 (2003). Medline doi:10.1126/science.1079567
2. B. Weber, S. Mahapatra, H. Ryu, S. Lee, A. Fuhrer, T. C. Reusch, D. L. Thompson, W. C. Lee, G. Klimeck, L. C. Hollenberg, M. Y. Simmons, Ohm's law survives to the atomic scale. *Science* **335**, 64–67 (2012). Medline doi:10.1126/science.1214319
3. Q. Xu, B. Schmidt, S. Pradhan, M. Lipson, Micrometre-scale silicon electro-optic modulator. *Nature* **435**, 325–327 (2005). Medline doi:10.1038/nature03569
4. L. Novotny, B. Hecht, *Principles of Nano-optics* (Cambridge Univ. Press, Cambridge, 2012).
5. A. L. Falk, F. H. L. Koppens, C. L. Yu, K. Kang, N. de Leon Snapp, A. V. Akimov, M.-H. Jo, M. D. Lukin, H. Park, Near-field electrical detection of optical plasmons and single-plasmon sources. *Nat. Phys.* **5**, 475–479 (2009). doi:10.1038/nphys1284
6. C. Henkel, S. Pötting, M. Wilkens, Loss and heating of particles in small and noisy traps. *Appl. Phys. B* **69**, 379–387 (1999). doi:10.1007/s003400050823
7. Y. J. Lin, I. Teper, C. Chin, V. Vuletić, Impact of the Casimir-Polder potential and Johnson noise on Bose-Einstein condensate stability near surfaces. *Phys. Rev. Lett.* **92**, 050404 (2004). Medline doi:10.1103/PhysRevLett.92.050404
8. M. P. A. Jones, C. J. Vale, D. Sahagun, B. V. Hall, E. A. Hinds, Spin coupling between cold atoms and the thermal fluctuations of a metal surface. *Phys. Rev. Lett.* **91**, 080401 (2003). Medline doi:10.1103/PhysRevLett.91.080401
9. D. Harber, J. McGuirk, J. Obrecht, E. Cornell, *J. Low Temp. Phys.* **133**, 229–238 (2003). doi:10.1023/A:1026084606385
10. M. Brownnutt, M. Kumph, P. Rabl, R. Blatt, Ion-trap measurements of electric-field noise near surfaces, http://arxiv.org/abs/1409.6572 (2014).
11. L. S. Langsjoen, A. Poudel, M. G. Vavilov, R. Joynt, Qubit relaxation from evanescent-wave Johnson noise. *Phys. Rev. A* **86**, 010301 (2012). doi:10.1103/PhysRevA.86.010301
12. C. Beenakker, H. van Houten, Quantum transport in semiconductor nanostructures. *Solid State Phys.* **44**, 1–228 (1991). doi:10.1016/S0081-1947(08)60091-0
13. S. Datta, *Electronic Transport in Mesoscopic Systems* (Cambridge Univ. Press, Cambridge, 1997).
14. A. C. Bleszynski-Jayich, W. E. Shanks, B. Peaudecerf, E. Ginossar, F. von Oppen, L. Glazman, J. G. Harris, Persistent currents in normal metal rings. *Science* **326**, 272–275 (2009). Medline doi:10.1126/science.1178139
15. H. Bluhm, N. C. Koshnick, J. A. Bert, M. E. Huber, K. A. Moler, Persistent currents in normal metal rings. *Phys. Rev. Lett.* **102**, 136802 (2009). Medline doi:10.1103/PhysRevLett.102.136802
16. D. Rothfuß, A. Reiser, A. Fleischmann, C. Enss, Noise thermometry at ultra low temperatures. *Appl. Phys. Lett.* **103**, 052605 (2013). doi:10.1063/1.4816760
17. L. Childress, M. V. Gurudev Dutt, J. M. Taylor, A. S. Zibrov, F. Jelezko, J. Wrachtrup, P. R. Hemmer, M. D. Lukin, Coherent dynamics of coupled electron

and nuclear spin qubits in diamond. *Science* **314**, 281–285 (2006). Medline doi:10.1126/science.1131871
18. J. R. Maze, P. L. Stanwix, J. S. Hodges, S. Hong, J. M. Taylor, P. Cappellaro, L. Jiang, M. V. Dutt, E. Togan, A. S. Zibrov, A. Yacoby, R. L. Walsworth, M. D. Lukin, Nanoscale magnetic sensing with an individual electronic spin in diamond. *Nature* **455**, 644–647 (2008). Medline doi:10.1038/nature07279
19. G. Balasubramanian, I. Y. Chan, R. Kolesov, M. Al-Hmoud, J. Tisler, C. Shin, C. Kim, A. Wojcik, P. R. Hemmer, A. Krueger, T. Hanke, A. Leitenstorfer, R. Bratschitsch, F. Jelezko, J. Wrachtrup, Nanoscale imaging magnetometry with diamond spins under ambient conditions. *Nature* **455**, 648–651 (2008). Medline doi:10.1038/nature07278
20. J. P. Tetienne, T. Hingant, J. V. Kim, L. H. Diez, J. P. Adam, K. Garcia, J. F. Roch, S. Rohart, A. Thiaville, D. Ravelosona, V. Jacques, Nanoscale imaging and control of domain-wall hopping with a nitrogen-vacancy center microscope. *Science* **344**, 1366–1369 (2014). Medline doi:10.1126/science.1250113
21. E. Schäfer-Nolte, L. Schlipf, M. Ternes, F. Reinhard, K. Kern, J. Wrachtrup, Tracking temperature dependent relaxation times of individual ferritin nanomagnets with a wide-band quantum spectrometer, http://arxiv.org/abs/1406.0362 (2014).
22. M. Pelliccione, B. A. Myers, L. Pascal, A. Das, A. C. Bleszynski Jayich, Two-dimensional nanoscale imaging of gadolinium spins via scanning probe relaxometry with a single spin in diamond, http://arxiv.org/abs/1409.2422 (2014).
23. Materials and methods are available as supporting material on *Science* Online.
24. T. H. Taminiau, J. Cramer, T. van der Sar, V. V. Dobrovitski, R. Hanson, Universal control and error correction in multi-qubit spin registers in diamond. *Nat. Nanotechnol.* **9**, 171–176 (2014). Medline doi:10.1038/nnano.2014.2
25. A. A. Baski, H. Fuchs, Epitaxial growth of silver on mica as studied by AFM and STM. *Surf. Sci.* **313**, 275–288 (1994). doi:10.1016/0039-6028(94)90048-5
26. J. H. Park, P. Ambwani, M. Manno, N. C. Lindquist, P. Nagpal, S. H. Oh, C. Leighton, D. J. Norris, Single-crystalline silver films for plasmonics. *Adv. Mater.* **24**, 3988–3992 (2012). Medline doi:10.1002/adma.201200812
27. G. W. Ford, W. Weber, Electromagnetic interactions of molecules with metal surfaces. *Phys. Rep.* **113**, 195–287 (1984). doi:10.1016/0370-1573(84)90098-X
28. N. W. Ashcroft, N. D. Mermin, *Solid State Physics* (Holt, Rinehart and Winston, New York, 1976).
29. P. Maher, L. Wang, Y. Gao, C. Forsythe, T. Taniguchi, K. Watanabe, D. Abanin, Z. Papić, P. Cadden-Zimansky, J. Hone, P. Kim, C. R. Dean, Tunable fractional quantum Hall phases in bilayer graphene. *Science* **345**, 61–64 (2014). Medline doi:10.1126/science.1252875
30. L. Faoro, L. B. Ioffe, Microscopic origin of low-frequency flux noise in josephson circuits. *Phys. Rev. Lett.* **100**, 227005 (2008). Medline doi:10.1103/PhysRevLett.100.227005
31. S. M. Anton, J. S. Birenbaum, S. R. O'Kelley, V. Bolkhovsky, D. A. Braje, G. Fitch, M. Neeley, G. C. Hilton, H. M. Cho, K. D. Irwin, F. C. Wellstood, W. D. Oliver, A. Shnirman, J. Clarke, Magnetic flux noise in dc SQUIDs: Temperature and geometry dependence. *Phys. Rev. Lett.* **110**, 147002 (2013). Medline doi:10.1103/PhysRevLett.110.147002
32. L. S. Langsjoen, A. Poudel, M. G. Vavilov, R. Joynt, Electromagnetic fluctuations near thin metallic films. *Phys. Rev. B* **89**, 115401 (2014). doi:10.1103/PhysRevB.89.115401
33. A. Jarmola, V. M. Acosta, K. Jensen, S. Chemerisov, D. Budker, Temperature- and magnetic-field-dependent longitudinal spin relaxation in nitrogen-vacancy ensembles in diamond. *Phys. Rev. Lett.* **108**, 197601 (2012). Medline doi:10.1103/PhysRevLett.108.197601
34. S. Pezzagna, B. Naydenov, F. Jelezko, J. Wrachtrup, J. Meijer, Creation efficiency of nitrogen-vacancy centres in diamond. *New J. Phys.* **12**, 065017 (2010). doi:10.1088/1367-2630/12/6/065017

ACKNOWLEDGMENTS

We thank Eugene Demler, Ania Jayich, Bryan Myers, Amir Yacoby, Maxim Vavilov, Robert Joynt, Amrit Poudel, and Luke Langsjoen for helpful discussions and insightful comments. Financial support was provided by the Center for Ultracold Atoms, the National Science Foundation (NSF), the Defense Advanced Research Projects Agency Quantum-Assisted Sensing and Readout program, the Air Force Office of Scientific Research Multidisciplinary University Research Initiative, and the Gordon and Betty Moore Foundation. S.K. and A.S. acknowledge financial support from the National Defense Science and Engineering Graduate fellowship, V.E.M. from the Society of Fellows of Harvard University, and S.K. from the NSF Graduate Research Fellowship. All fabrication and metrology was performed at the Center for Nanoscale Systems (CNS), a member of the National Nanotechnology Infrastructure Network, which is supported by the NSF under award no. ECS-0335765. The CNS is part of Harvard University.

SUPPLEMENTARY MATERIALS

www.sciencemag.org/cgi/content/full/science.aaa4298/DC1
Materials and Methods
Figs. S1 to S7
Tables S1 to S3
References (*32*–*34*)

4 December 2014; accepted 16 January 2015
Published online 29 January 2015
10.1126/science.aaa4298

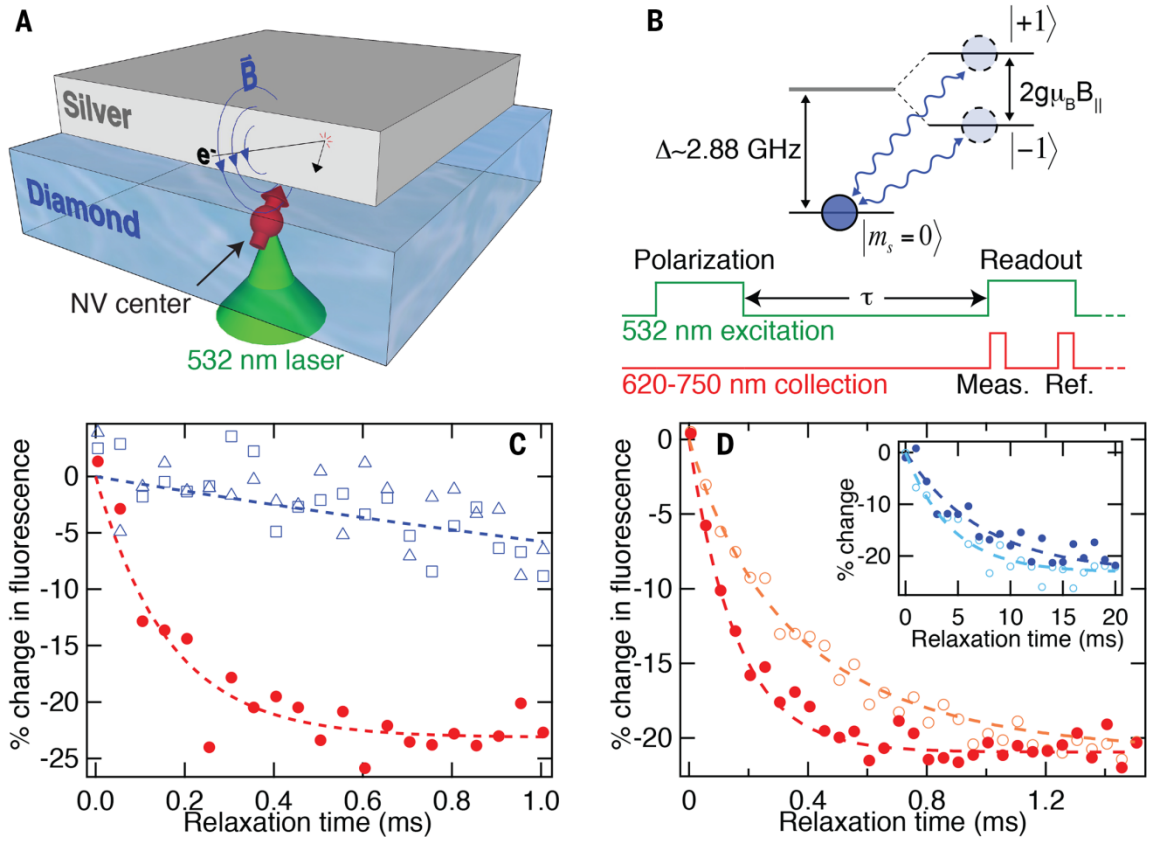

Fig. 1. Probing Johnson noise with single spin qubits. (**A**) The thermally induced motion of electrons in silver generates fluctuating magnetic fields ($\vec{B}$), which are detected using the spin of a single NV. The NV is polarized and read out through the back side of the diamond. (**B**) The NV spin is polarized into the $|ms=0\rangle$ state using a green laser pulse. Spin relaxation into the $|ms=\pm1\rangle$ states is induced by magnetic field noise at ~2.88 GHz. After wait time τ the population left in $\langle 0\rangle$ is read out by spin-dependent fluorescence. All measurements shown were performed at low magnetic fields ($\Delta \gg g\mu_B B_{\|}/\hbar$). (**C**) Spin relaxation data for the same single shallow implant NV before silver deposition (open blue squares), with silver deposited (red circles), and after the silver has been removed (open blue triangles). (**D**) Spin relaxation for a single NV close to a silver film prepared in the $|ms=0\rangle$ state (red circles), and in the $|ms=-1\rangle$ state (open orange circles). (Inset) Spin relaxation for a single native NV in bulk diamond in the $|ms=0\rangle$ state (blue circles), and in the $|ms=-1\rangle$ state (open light blue circles).

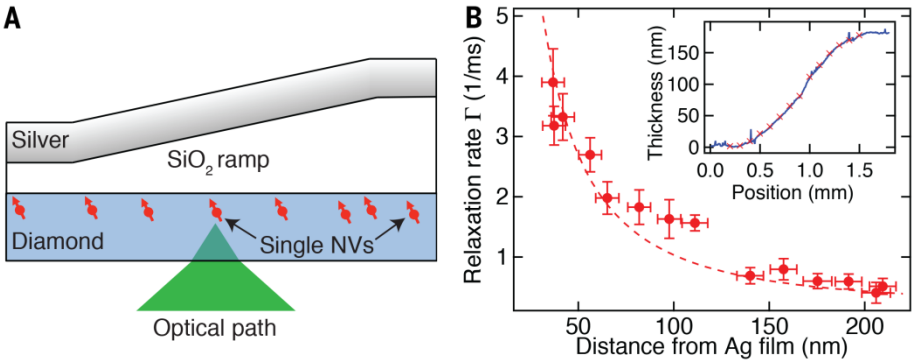

Fig. 2. Distance dependence of NV relaxation close to silver. (**A**) A gradual SiO_2 ramp (slope of ~.2 nm/micron) is grown on the diamond surface, followed by a 60 nm silver (Ag) film. (**B**) The NV relaxation rate is measured as a function of position along the ramp, which is then converted to distance to the film. At each point 5-10 NV centers are measured, and the minimum rate measured is plotted (red circles). The red dashed line shows the expected relaxation rate with no free parameters after accounting for the finite silver film thickness. (**Inset**) Thickness of the ramp as a function of lateral position along the diamond sample (blue curve). The red crosses correspond to the positions along the sample where the measurements were taken.

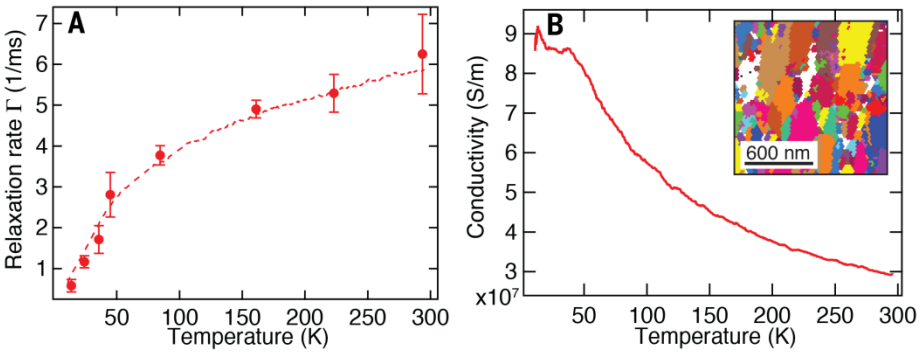

Fig. 3. Temperature dependence of NV relaxation close to polycrystalline silver. (**A**) The measured relaxation rate of a single NV spin under a polycrystalline silver film as a function of temperature (red data points). The conductivity of the silver film as a function of temperature shown in B is included in a fit to Eq. 2, with the distance to the film as the single free parameter (red dashed line). The extracted distance is 31±1 nm. (**B**) The conductivity of the 100 nm thick polycrystalline silver film deposited on the diamond surface is measured as a function of temperature. (**Inset**) Grain boundaries within the polycrystalline silver film, imaged using electron backscatter diffraction (EBSD). The average grain diameter is 140 nm, with a standard deviation of 80 nm.

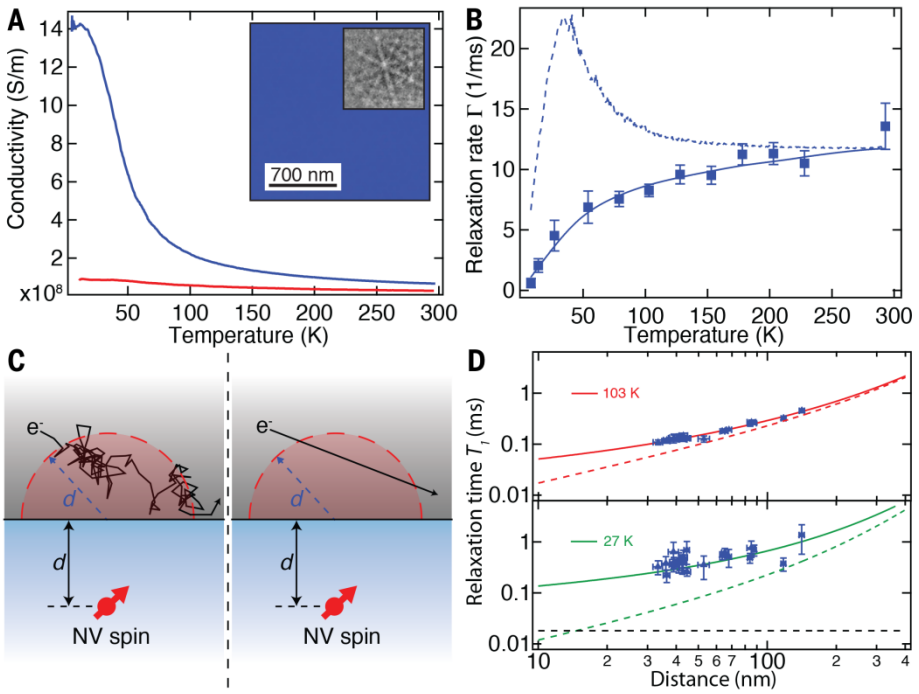

Fig. 4. Temperature dependence of NV relaxation close to single-crystal silver. (**A**) Measured conductivity of single-crystal (blue curve) and polycrystalline (red curve, same as Fig. 3B) silver as a function of temperature. (**Inset**) Electron backscatter diffraction image of the single-crystal silver film showing no grain boundaries, and the observed diffraction pattern. (**B**) Relaxation of a single NV spin under single-crystal silver as a function of temperature (blue squares). Equation 2 is fit to the data from 200-295 K (blue dashed line). A non-local model (23) is fit to the data (blue solid line), the extracted distance between the NV and the silver surface is 36 ± 1 nm. (**C**) Cartoon illustrating the relevant limits, where the noise is dominated by diffusive electron motion (left, $l \ll d$), and ballistic motion (right, $l \gg d$). (**D**) The same data as **B** was taken for 23 NVs at varying distances from the film. The T_1 of each NV at 103 K (top) and 27 K (bottom) is plotted against the extracted depth (blue triangles). The non-local model (solid colored lines) saturates at a finite lifetime determined by Eq. 3 (bottom, dashed black line), while the local model does not (dashed colored lines).